The University of Manchester

School of Electrical and Electronic Engineering

Embedded Systems Project

DESIGN REPORT #2

Title: Technical Characterisation

Group Number: 22

Group members name:	ID Number	I confirm that this is the group's own work.
Aarambh Sinha	10163290	☒
Abdullah Ahmed Akhtar	10059854	☒
Marlon A. Guanoluisa Pozo	10145373	☒
Osama Othman	10135442	☒
Subhi Alsous	9975113	☒

Tutor: Zhirin Hu

Date: 30/11/2018

Contents

1. Introduction

The primary goal of the project is to construct a microcontroller-based buggy in which various aspects are crucial and necessary for achieving the desired target. The main aim of the buggy is to mainly follow a white line which includes a number of diverse obstacles and challenges. These motivating challenges include, but are not limited to, slopes of maximum 18º, random line gaps of around 6 mm, vulnerability of track to direct sunlight and a tunnel with a 20 cm height. To assist tackling these problems and more, this report delivers the interesting design specifications across the different technical areas required. The aims of this report feed massively into the initial, main target of the entire project and provides the basis for construction and implementation.

The focal purpose of this document is to achieve the essential designs and implementation theories to progress to the next phase of the project. The aims include constructing the software specifications for the buggy to create a better, improved understanding of the system and what will it do exactly. Furthermore, an objective is to choose carefully the ideal line sensor out of the available options. This will be accompanied by the creation and design of the resulting circuit diagrams along with the PCB prototype. Also, focus will be applied on completing a plan that shows and demonstrates the control strategy that will be put in place for execution. The final intention or objective of this report is to generate a practical chassis design which is considered a key hardware component for the overall project.

The mentioned objectives relate closely to the main aims of the whole project in which the buggy creation could not proceed without taking a close look at the relevant sections within this report. To ensure satisfaction of the aims and targets, the report discusses in detail and analyses the following main topics: software, line-sensing, non-line sensing, control theory and hardware overview.

The first section takes a look at the general and specific requirements of the software, which addresses any constraints and the use of any case diagrams to help shape the overall system abilities. This is a requisite for the programming duty as it provides the necessary information to proceed with the coding in the next stage. Following on, the line-sensing part showcases the various possible sensor combinations and includes all required measurements and graphs. This section is responsible for choosing the line sensor which the circuit diagram and PCB design would be based on. Other relevant non-line sensors including encoders will be discussed briefly. Previous sensor choice lays out the foundation for the control section to discuss the proposed sensor set-up along with the most reasonable control algorithm. Finally, all previous sections will provide the components needed to deliver the optimum chassis design along a closer look at the hardware overview.

2. Software

2.1. Functional summary

When the autonomous buggy is switched on it will keep still until it detects a white line, then it will immediately turn on the motor and start rotating its wheels. Once it had started, it will be capable of autonomously follow the track without losing its stability and direction even when it goes through a ramp up to 18 degrees of inclination. If there is an end in the track, not a small gap, the buggy will instantly stop, if not, it will keep going.

However, if a rotation of 180 degrees of the buggy is desired, then there will be a system to perform this task. A Bluetooth Low Energy (BLE) will intervene to make the buggy turn around and return all the way back, of course, while a white line is present

2.2. List of possible software constraints

Lack of experience: From the begging of this project each member has been showing their strengths and weaknesses. Everyone has difficulties for programming, lack of experience using C++ and/or using mbed/low-level libraries, which could probably end with a buggy performing in a different way to the desired.

Memory capacity: The device used to execute the program will be the STM32F401RE which has a Flash memory of up to 512 Kbytes and a SRAM of up to 96 Kbytes. The code should not exceed these limits [1].

Time response: Another characteristic of the device mentioned before is its frequency. It can work with a frequency of up to 84Mhz according with its datasheet [1].

Program not loaded correctly: Some problems may be found when the program is tried to load to the STM32 board, this can be, it is no longer available to download the software to the board or the microcontroller not being found.

Context diagram

- SPT: Sensors for Perceiving the Track.
- SC: Sensors for Curving
- PRL: Position with respect to the line.
- PWM: Pulse wave modulation.
- M (R, L): Right Motor, Left Motor.
- BT: Battery Monitor

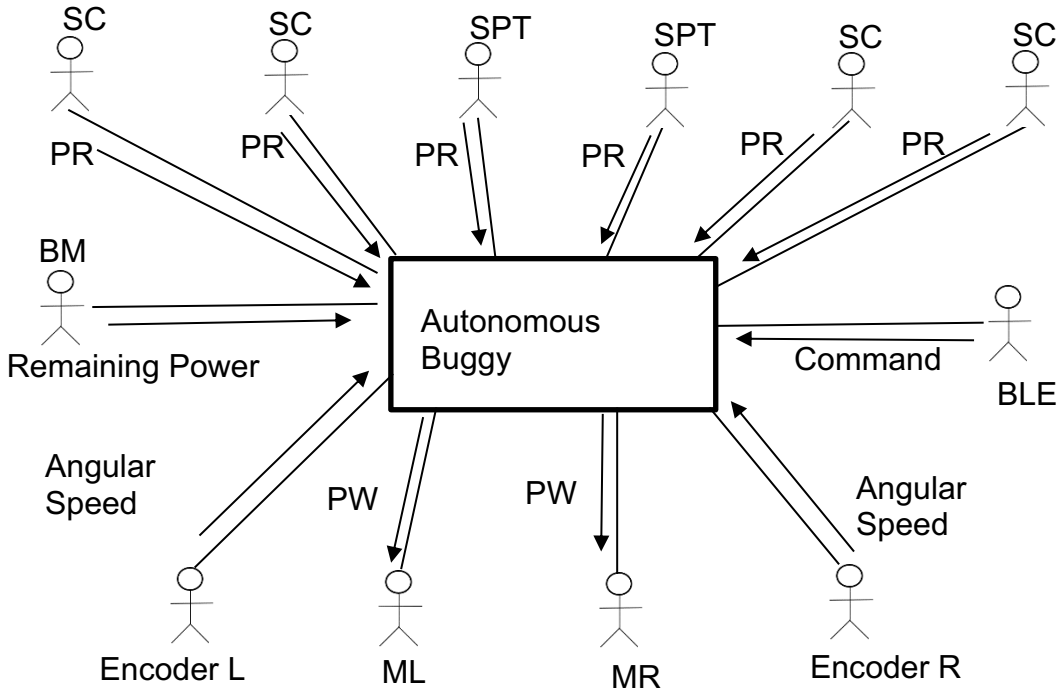

Figure 2.1Interaction between the external objects and the system.

2.3. Table of messages

Name	Description	Source	Destination	Interface	Size in bits	Arrival pattern	Comments
Position with respect to the line	Detects the changes between black and white	SPTs & SCs	System	SPI	TBD	TBD	Sensor TCRTR5000 will be used
Command	Receive the command to turn around	BLE	System	I^2C	20	Periodic 32 MHz	HM-10 Module will be used
Remaining Power	Estimate remaining run time	MB	System	SPI	10	TBD	DS2781
Angular Speed	Speed of the rotation about vertical axis	Encoders	System	SPI	TBD	TBD	Sensor AEAT-601B-F06 will be used
Pulse wave modulation	Pulse generated for rotating the motor	System	M (L, R)	SPI	TBD	TBD	None

Table 2.1 Capture information about messages.

Case Diagram

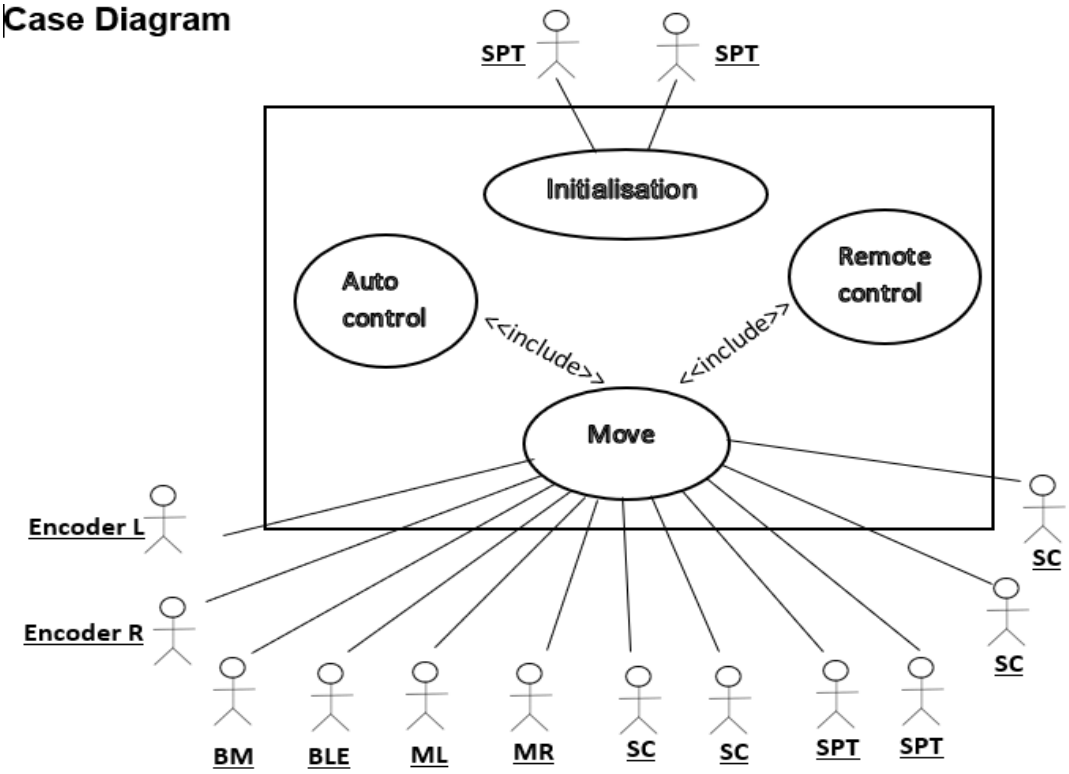

Figure 2.2 Messages exchanges between actors and system

2.4. Case Descriptions

INITIALISATION
Main Flow of events
Wait for **detection of white line** from **SPTs**
MOVE selected use case.
Alternative flow
IF **detection of white line** is not recived from **SPTs** then DO nothing.

MOVE
Main Flow of events
Wait for **position with respect to the line** from **SCs**
Wait for **speed of rotation** from **Encoders.**
Wait for **level of power** from **BM**
IF **command** is received from **BLE**
Start sending same **PWM** to **ML** and **MR**

Alternative flow 1
IF **position with respect to the line** is received from **SCs**
Increment and/or decrease the **PWM** of **ML** or **MR** depending of the **position with respect to the line**

Alternative flow 2
IF **command** is received from **BLE**
Deactivate **SCs**
Increment and/or decrease the **PWM** of **ML** or **MR** for turning around
INITIALISATION selected use case

Alternative flow 3
IF **level of power** is received from **BM**
Deactivate **SCs** and **SPTs**

2.5. Object specifications

```
WHILE NOT finished
    Wait for detection of white line
        While (detection of white line) {
            Input:
                Position with respect to the line from SPTs
                Position with respect to the line from SCs
                Angular speed from Encoders
                Command from BLE
                Remaining power from BM
            Execute control algorithm
            Output:
                PWM to MR
                PWM to ML
            }
            ELSE
            Finished=TRUE
```

3. Line Sensor Characterisation

3.1. Experimental Methods

To be able to effectively characterise individual emitter and receiver components, multiple key tests must be performed on every possible sensor combination. These tests allow the group to apply the technical information on datasheets to real world situations; such as monitoring output across different heights and the behaviour of the sensor when moving from black to a white path. The initial test, dark current, measures the current flowing across the transistor/diode/LDR at complete darkness when the emitter is switched off. While the TCRT5000 phototransistor shares its traits to an NPN bipolar junction transistor, the group noticed that even under zero illuminance conditions, there was a small current flow, this may be due to the depletion region still allowing the flow of electrons as it is impossible to achieve complete darkness.

	Dark Current (mA)	Background Illumination (mA)
TCRTR5000 Receiver	0.0072	0.0084
SFH203P	0.0000000739	0.0000794
VT90N2	0.0045	1.639
BPW17N	0.0000000212	0.00104

Table 3.1 Comparing current flow across receivers

Similarly, with background illumination, in order to create a standardised lighting condition, a phone torch was used by placing it a metre above the sensor. While this had very little effect on infrared photodiodes and transistors, the potential difference across the LDR showed a considerable difference.

The experimental methods of the line-spread and height variation measurements involved using a test rig with slots separated every 5 mm. The sensors were attached to an 8 pin DIL socket in a circuit mounted to a stripboard. This stripboard could be slid into individual slots. This ensured the test sensors would be measured across the same heights and horizontal positions on the test platform (white tape on a black plastic).

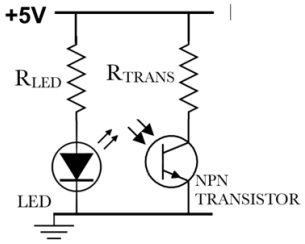

$$I_{receiver} = \frac{V_{resistor}}{R_{resistor}} \quad (3.1)$$

$$P_{component} = V_{power\ supply} . I_{component} \quad (3.2)$$

Figure 3.1 A snapshot of a schematic diagram showing how both emitter and receiver and connected.

The results are reproducible as the measurements can be taken using the testing rig and mounting the sensors onto the stripboard. Ensuring that using a power supply with sufficient current and electromotive force output is important as individual sensors draw on specific amounts of current. To keep the data consistent, the same power supply was used across all sensors with calculations to confirm that the current would not be exceeding 100 mA on the MyDAQ.

The following current flow across different sensors were measured by reading the

voltage across the resistor connected in series to the sensors. As the resistance of the photodiodes/phototransistor/LDR is unknown and dependent on the conditions, measuring the potential difference across the resistor, followed by dividing by the resistor value, finds the current flow across the branch.

Sensor Characteristics

	Type	Wave-length range	Peak λ (nm)	Affected by Sunlight	Resistor in Series (ohm)	Capacitance
TCRT5000	Photo-transistor	NA	NA	No	10000	NA
SFH203P	Photodiode	550-1050	840	No	470,000	11 pF
VT90N2	LDR	500-650	550	Yes	8170	2.49 uF
BPW17N	Photo-transistor	450-1040	825	No	100,000	8 pF
TCRT5000	LED IR	940-960	950	-	100	17 pF
OVL5521	LED Visible	“White”	-	-	62	-
OPE5685	LED IR	825-875	850	-	33	20 pF

Table 3.2 Showing characteristics of a range of emitters and receivers.

By reviewing the technical datasheet, a decision was made to test 5 different combination of sensors. Starting with infrared emitters and sensors, the OPE5685 and BPW17N showed characteristics that would be similar to TCRT5000 as both combinations use a phototransistor [15]. These phototransistors work effectively in the infrared region of wavelengths and the background illumination tests confirmed that the effect of sunlight would produce a negligible amount of noise that could affect the effectiveness of the sensors.

3.2. Emitter and Detector Pairing

Similarly, the OPE5685 was paired with the SFH203P photodiode. As the photodiode consists of a PN junction [14], one of the quirks of the photodiode was to place it in reverse polarity to the current flow. The SFH203P also is effective towards infrared wavelengths which would make it a sensible pairing with the OPE5685.

Other than infrared sensors, a visible light emitting sensor involved the OVL5521 and VT90N2. As the datasheets define both components to be effective in visible light [9]. An immediate disadvantage of this combination would involve the ambient brightness of the room changing the effectiveness of the sensor. The background illumination tests suggest that even applying a source of light a meter away from the LDR seemed to increase the noise in value of the potential difference across the resistor connected in series to the LDR. Despite analysing the lack of effectiveness of testing OPE5685 with VT90N2, this combination was chosen to confirm the hypothesis that infrared emitters would not perform as well with visible light detectors.

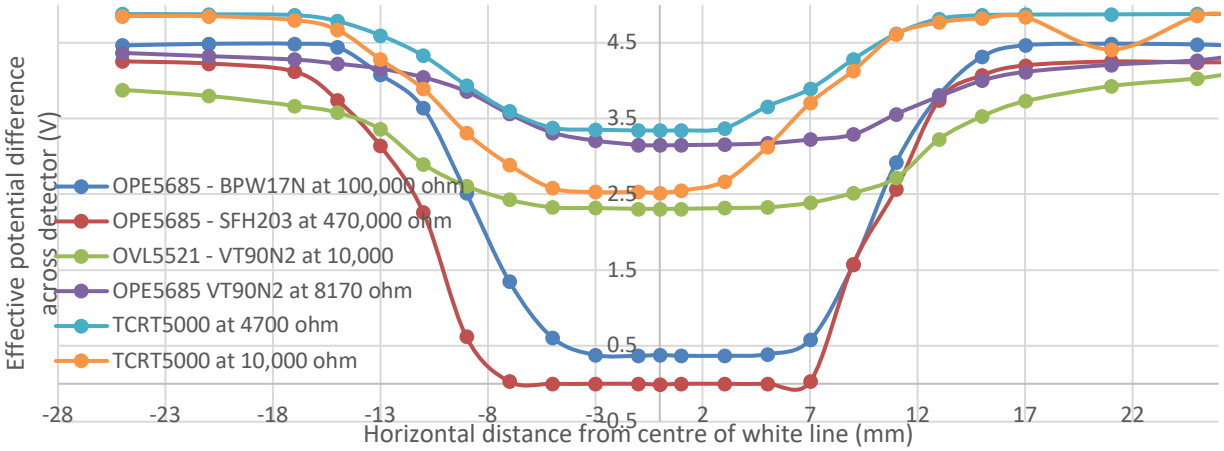

Figure 3.2A graph showing the effective voltage drop across the receiver components.

Comparing the line-spread characteristics of multiple sensors, where -9 and +9 mm are the edges of the white tape, the OVL5521-VT90N2 and OPE5685-VT90N2 clearly suggest a very limited dynamic range of voltage outputs. While both sets of data had taken background illumination voltage into consideration and negated ambient noise, the voltage drop across the LDR is still 3.88 V, comparing this to TCRT5000's voltage drop of 4.85 V at -28 mm from the centre of the line suggested that the TCRT5000 has a greater dynamic range of comparing white to black. While OPE5685-SFH203P and OPE5685-BPW17N showed very similar behaviour, there is a shallower gradient due to a greater variation. This could perhaps be due to OPE5685's greater angular displacement [7]. As the infrared light waves will be dispersed to a greater area, the precision of the OPE5685 would be limited as it would illuminate a larger surface area than the OVL5521. The TCRT5000 performs consistently with measurements and seems to reject noise signals fairly well. While the TCRT5000 only displays 3% of noise at the point where its furthest away from the centre of the line, the other sensor combinations have over 11.7% of noise that skew the measurements vertically. While the VT90N2 is not designed to be detect infrared wavelengths, it does produce a weakly distinguishable reading that is comparable to the visible light emitter.

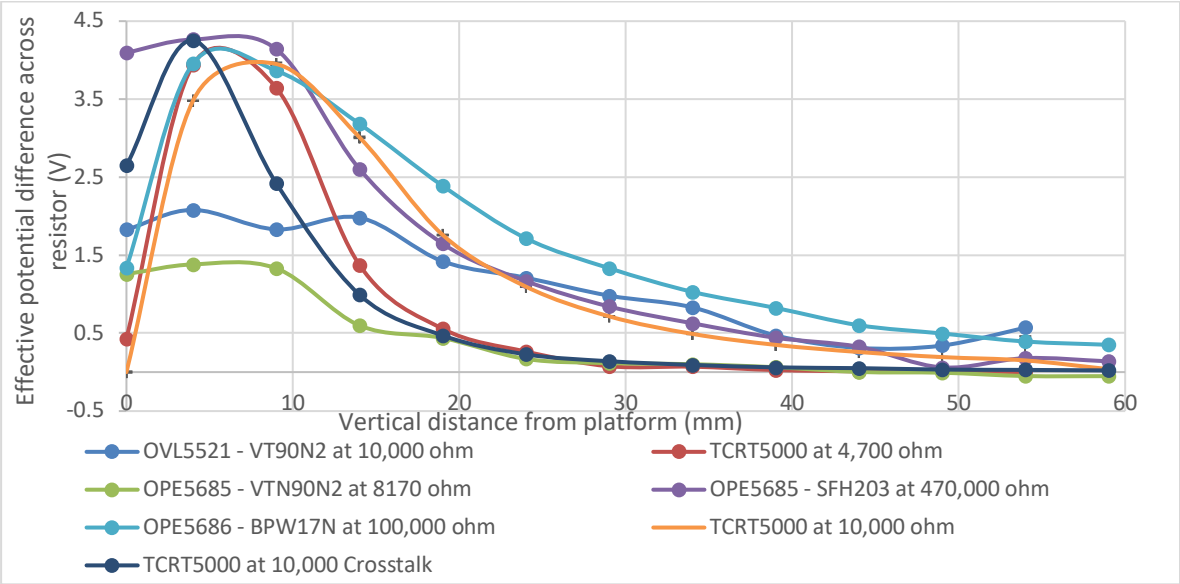

Figure 3.3 A graph comparing the effective voltage difference of sensors at varying heights.

The use of term ‘effective’ compares the potential difference across sensors between the white and black surfaces. To find the effective voltage difference, every data point in the graph reads the value of the resistor when the sensor is on white and negates the dark voltage and voltage when the sensor is on white.

From figure 3.3, the OPE5685 and VT90N2 combination outputs the least effective voltage differences compared to other combinations. While the sensor combination does show a weak correlation of distance to effective voltage, the effect of ambient light and electrical noise renders the sensor useless after 14 mm. Similarly, the OVL5521 and VT90N2 performs slightly better but has the same shortcomings. This is a clear indication that using an analogue device like an LDR does not provide a stark enough contrast in measurements to be used in this situation. While the SFH203P receiver produces a correlation that is comparable to the TCRT5000 and BPW17N, there was an extended period of time for the measurement to stabilise. This may be due to the high value of the resistor connected to the receiver. With a capacitance of 11 pF [12] and resistance of 470,000 ohms, it has a time constant that is 5 times longer than BPW17N at 100,000 ohms. The SFH203P is therefore 5 times slow at reading true values making it difficult to implement on a fast-moving buggy.

3.3. Choosing Preferred Sensor

The group chose the TCRT5000 as the preferred sensor due to its smaller footprint, accurately spaced emitter and detector and its consistent results. Comparing the two sets of measurements, the 10,000 ohm resistor performs better as it is able to discern the line over a greater distance than the 4,700 ohm combination.

Reviewing the measurements of the TCRT5000 with another TCRT5000 approximately 10 mm away from the receiver, there is a negative skew that causes the effective voltage difference to decline with a higher gradient. This could be explained due to negating the higher background illumination that is a result of both LEDs being turned on. This would suggest

specifying that no adjacent emitters must be switched on at the same time to avoid crosstalk in measurements.

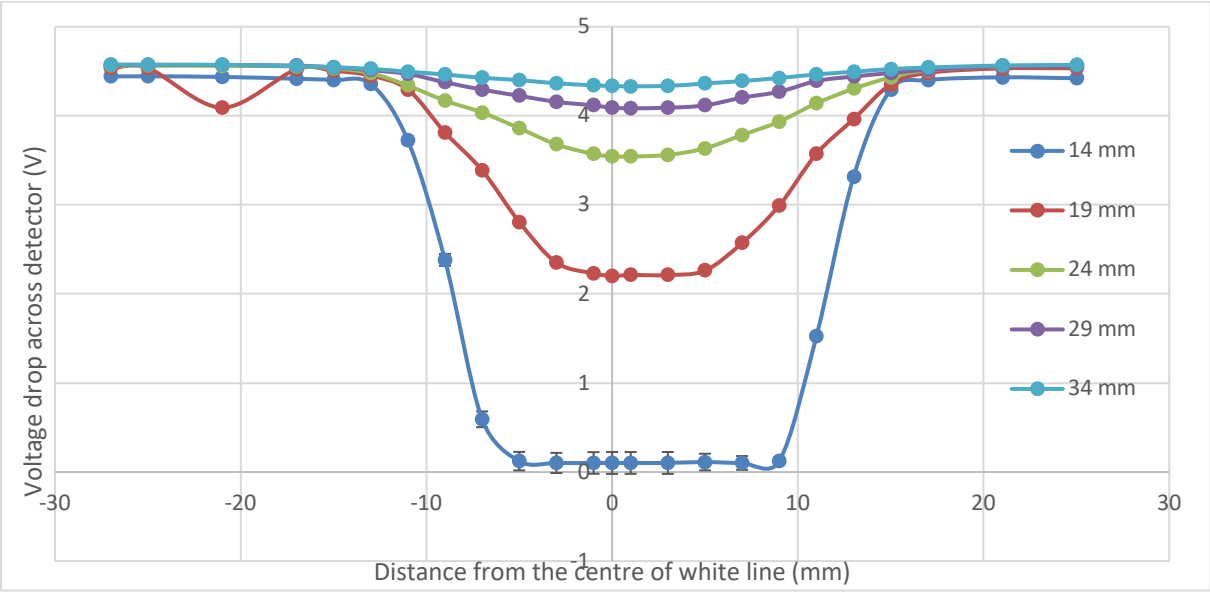

Figure 3.4 A graph comparing line-spread of TCRT5000 at 10,000 ohms across different heights.

3.4. Error Bars

As the measurements of the TCRT5000 were repeated 5 times, the average of all measurements was taken and plotted. The error bars are plotted by finding the difference between the highest value of the reading and average. The same is calculated for the minimum value and average. Figure 3.4 suggests a greater variation in measurements as the voltage drop increases. Figure 3.3 shows the variation being so small that the error bars not visible.

Upper bound : = (MAX(TEST1:TEST5) – AVERAGE(TEST1:TEST5))

Lower bound : = ((AVERAGE(TEST1:TEST5) – MIN(TEST1:TEST5))

4. Circuit diagram for proposed line sensors

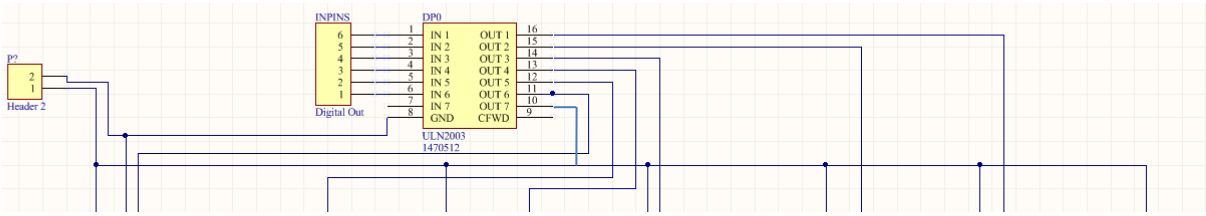

Figure 4.1 Section of schematic showing input signals of the sensor board.

Choosing the method of implementation and sensor configuration is justified in Control. The group decided to implement digital sensors. This means the sensor board will be interfacing with the microcontroller using digital inputs and outputs. As these DIO pins are limited to 5 V 4 mA, this is insufficient power to power the LEDs. The LEDs will therefore be powered by power rails from the motor driver board. A 7n element Darlington Pair chip ULN2003A is being used which will allow both independent control of LEDs and also provide the LEDs with sufficient current to be powered on. Pins 1 to 6 of the Darlington Pair are connected to the Digital Out pins from the microcontroller. The Darlington Pair is powered by the driver board to pin 10. The following pins 11 to 16 are connected to each individual LEDs. The transistors can be connected directly to the driver board as they do not draw as much current as the LEDs.

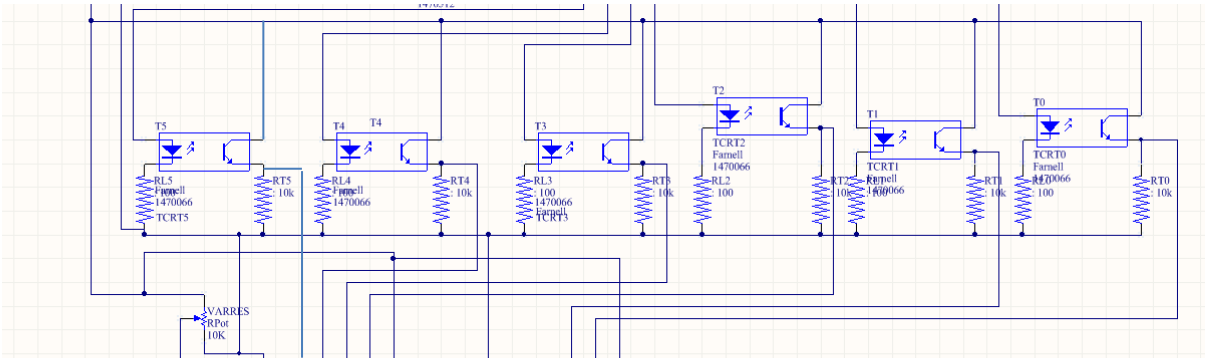

Figure 4.2 Section of schematic showing how LEDs, transistors and resistors connected.

The LEDs are in series with a 100 ohm resistor. These therefore connect to ground. The transistors are connected to a 10,000 ohm resistor (refer to 3.3). The comparator must measure across the resistor and ground.

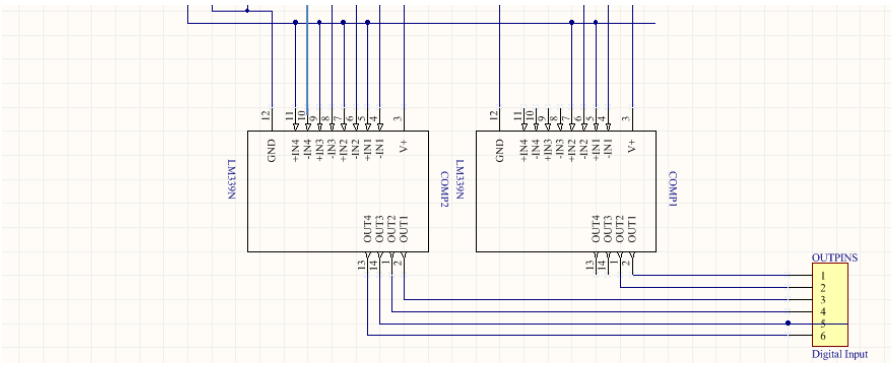

Figure 4.3 Section of schematic showing how analogue signals are converted to digital.

Due to decisions met in 6.4, the sensors must output digital signals from the sensor board. These signals can only be read in digital by the microcontroller so physical comparators are used to make the on/off decision on a hardware level. This decision allows the code to be simplified as no comparisons need to be made on a software level, inherently increasing the rate of sampling. The threshold of sensitivity can be determined by an analogue source (variable resistor) as this allows fine tuning on the race day without having to interfere with code. A 100,000 ohm maximum resistance value was chosen as the internal resistance of the comparator input is 5100 ohm [14] allowing the maximum threshold voltage to be set to 4.76 V.

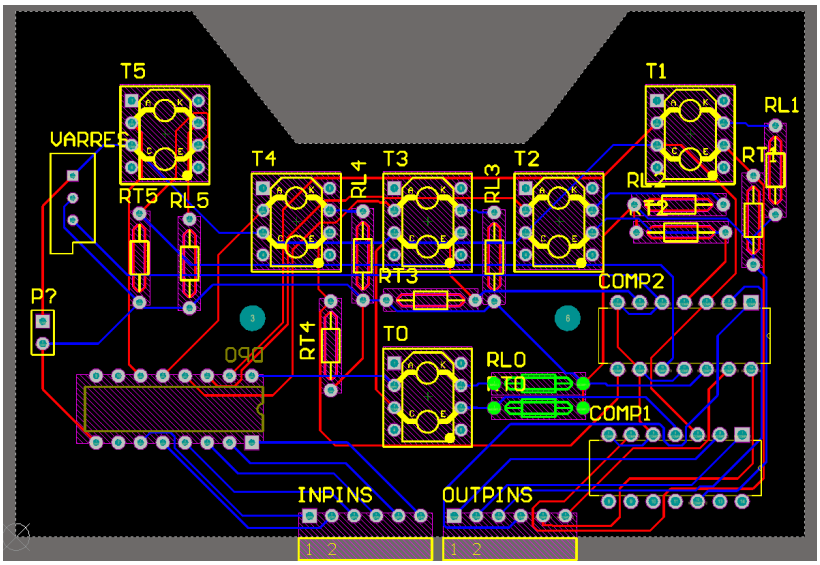

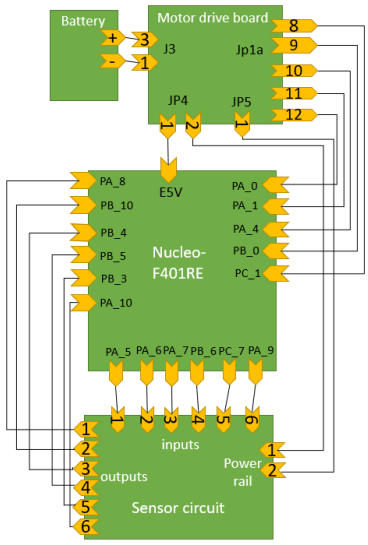

Figure 4.4 Block diagram showing how all peripherals interface with microcontroller [1] (see right)

Figure 4.5 Compiled schematic file to PCB using Altium Designer [16] (see left)

With constraints decided by the chassis design, the dimensions of the sensor board were defined. The trapezium cut out at the top is designed to have sufficient space for the castor wheel (see 7.2). The positions of the sensors are followed by the decisions made in section 6.5. The rest of the design focuses on the efficiency of routing and minimising any overlap in routing. The design implements a double layer copper contact profile with components placed on both sides to simplify layout of components.

4.1. Peripherals Interface

The battery will connect to the motor drive board using a 3 – way Molex connector. The current sensing voltage outputs, pins 9 to 12 of Jp1a will be outputted to the Nucleo ADC enabled I/O inputs to convert the analog voltage. Pin 8 of jp1a doesn't need an ADC input as it outputs binary information but to keep the 5 wires together it is inputted into ADC enabled input. To provide power to the Nucleo board a 5 V 600 mA J3 pin 1 output feeds into the E5V pin where power can be inputted using a I/O pin [23,24,29]. The sensors I/O outputs from the micro don't need to be ADC enabled as they need logic signals to control the Darlington pairs. As for the sensor outputs, a comparator circuit outputs logic 0 and 1 signals so these will also be normal I/O inputs. Finally, the Digital I/O cannot output more than 4 mA and one TCRT5000 transistor needs 38 mA so we use the +5V of motor drive board which offers 600 mA where the micro will take a max of 500 mA so 100 mA is more than enough to power everything [28,29].

5. Non-line sensors:

5.1. Speed Sensors

The AEAT-601B-F06 measures motion and direction by using two magnetic sensors that measure change across a disk and is included with the motor. When there's movement, if a rising edge is detected and count is incremented. This allows the measurement of wheel speed using the counts per second. The detection of direction uses two sensors, A and B, that are placed so that when there's motion, they detect a rising edge at a 90 ° phase difference. A will detect first when there's anticlockwise movement and B will detect first when there's clockwise movement. To use the quadrature interface mode, pin PA_5 and pin PB_3 will be used to input channel A and B, 5V connected to +5V and GND to GND both on CN6 and the index is not needed so it will remain disconnected [19,20]. The TIM 2 timer peripheral will increment the CNT register every rising edge without disrupting the CPU and we use a software timed interrupt to sample the number of counts every specified period to get the count rate. This can be used to calculate $\omega\,(rad.s^{-1})$, angular speed using the counts per revolution, where then ω can then be used to calculate wheel speed in $m.s^{-1}$ using wheel radius and gear ratio.

5.2. Motor Current Sensor

The motor drive board has a current sensing circuit that is used to input voltage across a 0.1 Ω resistor, in series with the motors, into the microcontroller for measurement [21]. First, The APLC-784 will amplify the voltage of this resistor using the isense+ and isense- paths. The gain being determined by VDDin of the amplifier which is fixed by the voltage regulator LM3480 – 5 at 5 V if the voltage input is above 6 V [22], to get a gain of 8.029 in order to get an output in the range of 0 – 5 V for currents of 0 – 1.4 A. The microcontroller will receive these measurements through Analog in pins Pin 10 Avago A(+) of jp1a to PB_0 and Pin 9 Avago A(–) of jp1a to PA_4 for Motor right, Pin 12 Avago B+ of jp1a to PA_0 and Pin 11 Avago B- of jp1a to PA_1 for Motor left [23,24].To get an accurate relationship constant between voltage and current, we have to collect data of current through motor turned on using an Ammeter and voltage using a volt meter across TP20 and TP18 for motor 1 for example, plot it and find the gradient. The software can then calculate the motor current from voltage input multiplying the gradient by input voltage.

5.3. Battery Monitoring

The DS2781 chip will measure the current and voltage from the battery, place it in a register and output it to the microcontroller upon a software command. The current is measured across the 0.01 Ω resistor called Rsns, and the voltage is measured at Vin, where voltage of battery is inputted to ground [25]. The voltage is measured down to a resolution of 9.76 mV and up to a maximum of +9.9902 V and the 10-bit voltage register is updated every 440 ms [25]. The chip is capable of reading the current down to a resolution of 1.56 μV/Rsns, therefore the resolution is 156 μA, and up to a maximum of +- 5.11 A as 16 bits are used for current measurement with the current measurement is updated every 3.515 s. The microcontroller Digital in PB_8 pin will connect to drive board pin 8 of Jp1a [23,24]. So, Using the DS2781 and the one wire method classes, software can read in the battery current and voltage.

5.4. Bluetooth Low Energy

The HM – 10 is a BLE module that allows the microcontroller to connect to other BLEs using a unique service profile the HM-10 in which is a collection of services with different purposes. The HM-10 capabilities include the ability to run at very high speeds of 32 MHz, allow both Slave and Master roles, send 20-bit character words ie. Hello would be 5 characters and can be put in sleep mode when not in use where it consumes much less power [26]. The HM-10's ability to act as slave allows the buggy to be controlled from another and only one BLE, our phones, that will be master to send a command to be processed by software of the microcontroller. To control the BLE in software, we use AT commands. The HM – 10 uses 32-bit AT commands that are sent to the module by software serially through the UART strip and software can then control the module using SoftSerial.h [27]. To connect the HM-10 to the STM32, CN6 3.3 V to VCC, CN6 GND to GND, PA_2 to TX and PA_3 to RX are used [26,24].

6. Control

Following the inspection and assessment of the various sensor measurements and characteristics, an algorithm is required to control the system in the most ideal manner. Firstly, before applying control, a method of capturing information regarding the exact position of the white line is necessary. In this case, the chosen TCRT5000 optical sensor is responsible for this operation using its infrared emitter and phototransistor detector. Basically, the led emits infrared radiation that's only reflected off a white surface back to the detector. The detector outputs a high voltage or a low voltage depending on the surface the sensor is positioned over directly. Multiple sensors aid the whole process which will be discussed later.

In terms of wheel control, a method is essential to ensure buggy movement occurs in both the right direction and speed. The direction is controlled using the H-bridge circuit embedded within the motor drive board in which a unipolar or bipolar mode is chosen. The choice is implemented by driving the digital output pin on the Nucleo board to operate in either modes. Wheel speed control is executed using a pulse width modulation (PWM) signal for each wheel separately. The PWM is configured depending on the sensor feedback which in return controls the duty cycle for each motor connected to each wheel. The resulting output is a constant, increase or decrease in each wheel's speed to direct the buggy back on track.

6.1. Proportional vs Bang-Bang

In terms of control, Proportional and bang-bang algorithms are two theories which represent different approaches and demonstrate dissimilar functionality. A bang-bang controller switches severely between on and off states which could be very useful in certain situations where a quick, abrupt reaction is mandatory, as in the case of brakes. In other instances, bang-bang largely limits the flexibility of a system forbidding any inter-state regions. Looking at programming, bang-bang is simpler to implement and work with compared to the Proportional controller. For the Proportional controller, the control is more reliable as it illustrates greater accuracy and precision. Error is dealt with a better handling that gives rise to a smoother, desired output. Drawbacks could be the complexity of the program and the lateness of response in toggling environments.

6.2. P, I and D in PID controllers

A practical method of implementing continuous control is a proportional-integral-derivative controller. Each term in the PID controller adds a specific functionality and could be advantageous or not depending on the certain situation or system. In general, the P corrects current error, the Integral looks at previous errors and the derivative predicts future errors.

The P term allows the controller to maintain stability of process by decreasing the error under steady state. However, the error is not entirely eliminated, and amplification of background noise is considered a main flaw. When minimal conditions are met, and system is lenient with steady state error, P controllers work greatly. The integral term solves the issue of the steady state error by rejecting and excluding it completely. This works at the optimum when the error margin is small, and the integral builds up a memory of all these deviations. However, if huge errors are continual, the integral could respond undesirably by overshooting in the opposite side in order to counter the large error. In terms of speed, the integral takes time to build up and so could affect negatively if quick motion is a requirement. The final term, the derivative, has the effect of predicting future errors and so is advantageous when speed is needed. A useful application is when the error is better than the previous one in which the derivative makes sure nothing is made to correct the error. Although it works well to prevent immediate deviations, the derivative amplifies the noise directly causing problems if used as PD controller [17].

6.3. Control strategy for each problem

A number of variables and components will have to controlled to influence the nature of the control algorithm. The direction and speed of the buggy movement form the basis of the control theory needed for implementation. Controlling the wheel direction works by controlling the motor through the drive board electronics. This is performed by the h-bridge circuit in which a unipolar mode is a superior operation, in this case, to reduce the power loss problems through lower conduction losses. On the other side, a PID controlling algorithm would help with the wheel direction control by increasing the accuracy of the line-sensing movement. This method overcomes the problem associated with the ban-bang controller in which the zig-zag movement is eliminated, and increased smoothness is outputted.

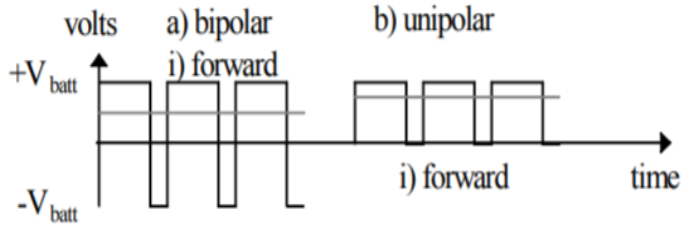

Figure 6.1 shows both unipolar and bipolar modes in forward direction

Figure 6.1 shows the unipolar signal varies between 0 V and ±V batt instead of the complete amplitude in both sides which ensures less switching power loss.

Another variable to be controlled is the wheel speed which is performed by controlling the motor linked to that wheel. The value of the PWM applied to each motor depends on what speed is needed to maintain track guidance. This is done by referring to the light sensor values along with the current wheel speed given by the encoders discussed in section 5.

6.4. Algorithm's relation to sensor design

Several control strategies could be implemented depending on the available sensor characteristics and behaviour. Different controllers operate ideally with different sensor designs and vice versa. Digital control works better with certain line sensors that demonstrate abrupt change in voltage measured when moving from black to white, in this case. On the other side, sensors that inhabit a very wide line spread function could work well with analogue control, improving accuracy. Moreover, bang-bang controllers adapt well when few sensors are used, limiting further functionality. However, PID controllers demonstrate their strengths when higher numbers of sensors are used to interpret the error better. These factors illustrate the close, direct relationship between the choice of control and the sensor model.

The choice of digital or analogue control affects the sensor set-up as the positioning of the middle light sensors depends heavily on it. For the digital implementation, the two middle sensors' ideal position is at the centre of the white line to feedback the highest voltage whereas others give back nearly 0 V. In terms of analogue, the alignment of the two middle sensors right about the white-black edge helps measuring the relevance of the buggy to the white track. For the microcontroller interface, the number of sensors used affect how many pins are needed. Furthermore, the switching between the various sensors' readings could require the use of a Darlington pair and comparators which affects the sensor circuit design.

6.5. Proposed sensor implementation

Following the previous discussed factors, the chosen line sensing set-up is composed of 6 TCRT5000 optical sensors. The sensor type is chosen based on the high white line detection accuracy compared to the other available measured line sensors. The performance of the TCRT5000 allows it to stand out as it's line spread function and crosstalk graphs support the PID and digital controlling theory. In terms of the number geometry, higher number of sensors used increase the line detection accuracy of the buggy. As the sensor inputs an analogue value into the microcontroller, an two comparators are responsible for the analogue-digital conversion. From figure 3.4 above, the threshold voltage is set as 4.398 V as to any sensor value below that suggest the sensor is above a black area and is given a logic level '0'. Above that

value, logic level is '1' and this implies the specific sensor is directly above the white line. For the microcontroller interface, 6 Digital Inputs will be used for the 6 line sensors. Figures 6.2 and 6.3 below show the sensor set-up over various track positions, implementation is justified based on the planned digital control approach.

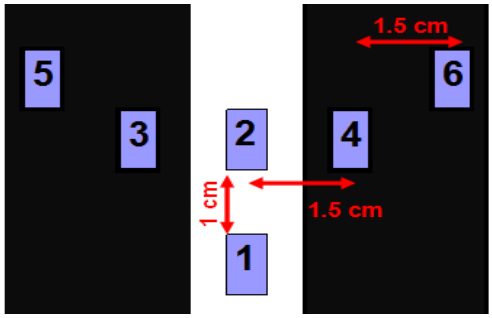

Figure 6.2 sensor set-up over straight

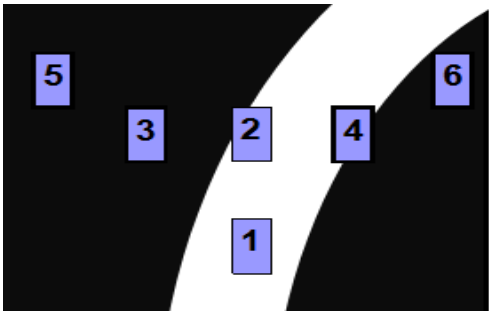

Figure 6.3 sensor set-up over gentle curve

6.6. Control implementation plan

To initialise the control, the first step is to ensure straight movement occurs when both sensors 1 and 2 return '1' while others return '0'. This is shown in figure 6.2, where an application of equal PWM of around 50% duty cycle on both motors resolves the issue. Building on that, bends of maximum 45º provide a control complication, illustrated in figure 6.3. Assuming a right curve as above, a gentle bend is detected by sensor 4 as well as sensors 1 and 2, in which a PWM of 50% maintains on the left wheel, however, the right wheel's PWM is reduced to 20% duty cycle to slow it down and aid slight right turn. In the race, a possible great bend requires a 30% PWM on the left wheel with 0% level or even braking on the right wheel [17]. This is applied following the feedback of logic level '1' from sensor 6 along sensors 1,2 and 4. All previous strategy will be implemented for the left turning with correspondence with the opposite wheels and sensors. To ensure smoothness of the above strategy, a PID controller will be used for error elimination with assessment of current, past and future errors. The controller, programmed in C++, will be positioned as in figure 6.4 below where the controller will be used to improve the sensing accuracy. Tuning of the controller will follow the Ziegler–Nichols method, with extra modification, to get the K_P, K_i and K_D constants required.

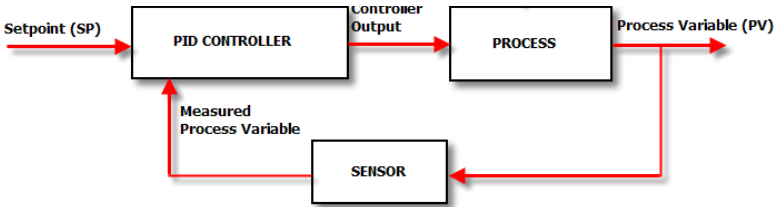

Figure 6.4 Control process overview [18]

In dealing with direct sunlight, the TCRT5000 have no problems as the sensors will be taped and covered to avoid outer influence. Finally, regarding the line breaks within the track, sensors 1 and 2 are distanced 1 cm apart to ensure the 6 mm gaps are irrelevant.

7. Hardware Overview

7.1. 2D drawings of Chassis

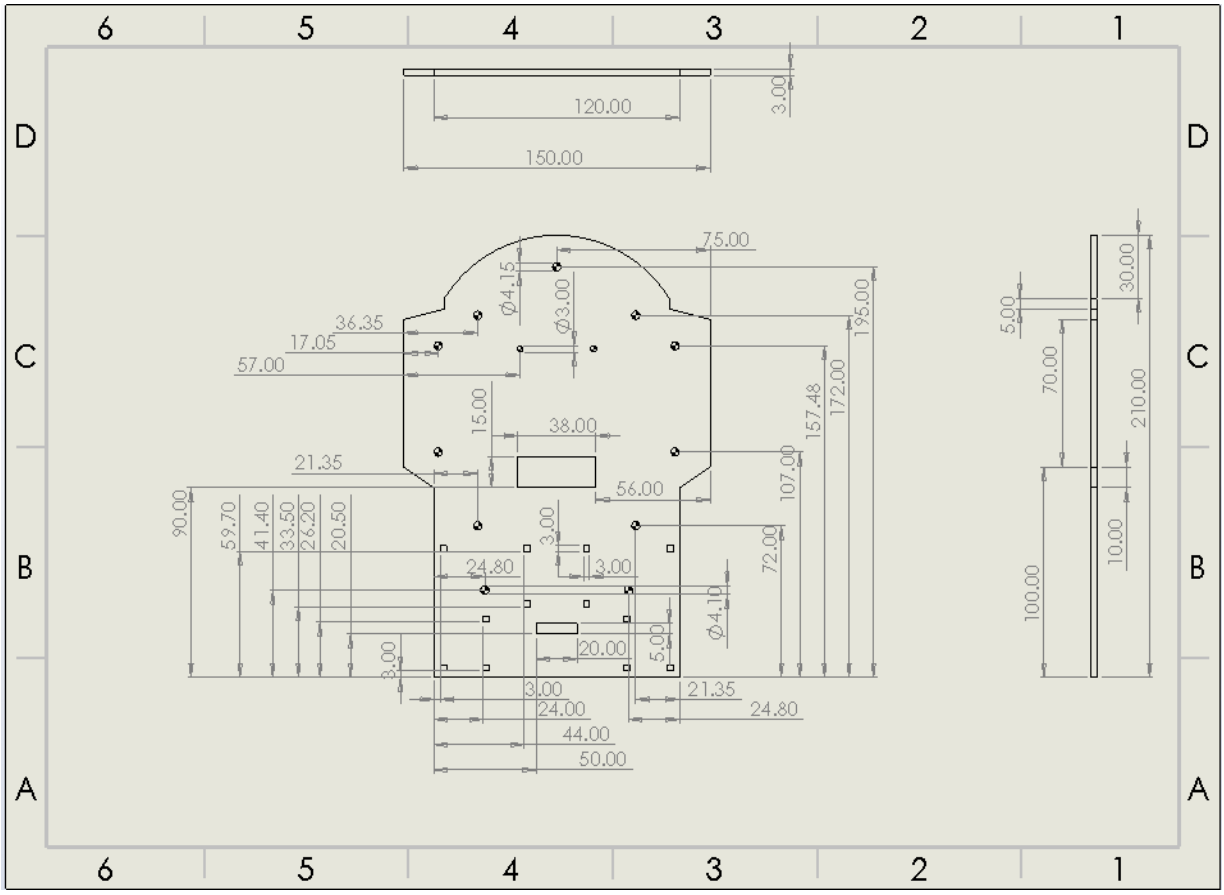

Figure 7.1 drawing of bottom plate [4]

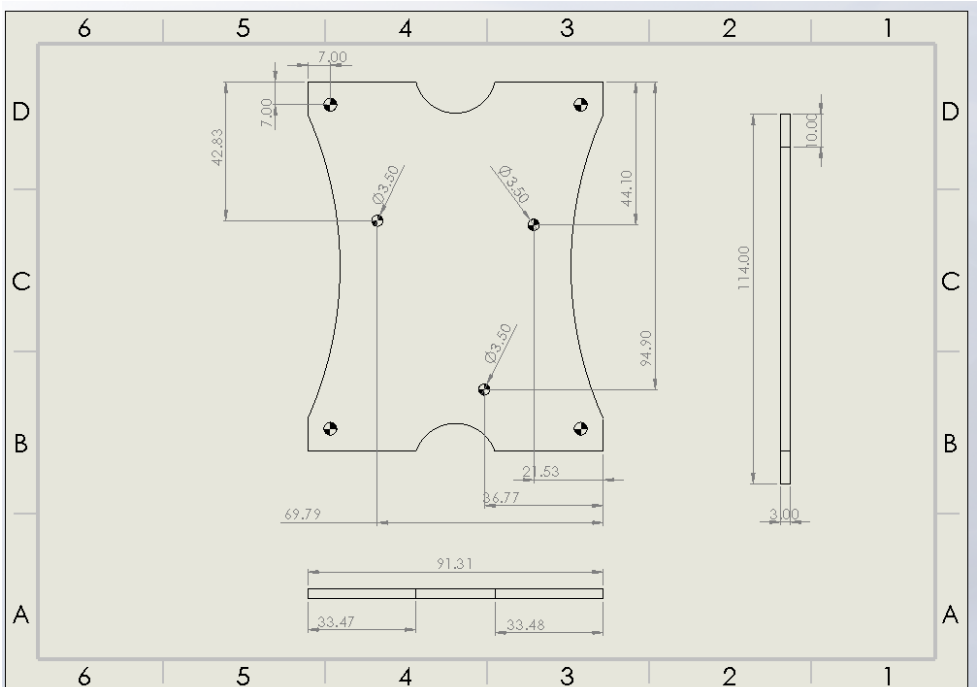

Figure 7.2 drawing of top plate [4]

All dimensions are in mm.

Scale for bottom plate is A4 landscape 1:2.

Scale for top plate is A4 landscape 1:1.

Holes without dimensions are 4mm in diameter.

7.2. Material Choice and Ease of Manufacture

In order to choose the material that is to be used for the chassis, comparisons should be made between the properties of the materials. The table of the different materials that were researched are shown below:

Table 7.1 Material properties[5]

Material Characteristics	Acetal	Glass-Reinforced Laminate	Aluminium	Mild steel
Density (Mg/m^2)	1.8	1.9	2.7	7.8
Flexural strength (MPa)	91	255	310	414
Ultimate Tensile Strength (MPa)	67	175	310	414
Young's Modulus (GPa)	2.8	11.5	69	207

The three main factors to be considered for chassis material are:

Weight: As can be seen in the table, acetal has the lowest density, while mild steel has the highest of all the materials. The material from which the chassis is cut must not be too dense in order to ensure that the buggy is not too heavy

Cost: In terms of material cost, aluminium is the most expensive and other three materials are similar in cost however cost of manufacturing is higher for steel and aluminium compared to acetal as it is harder to cut metals in shape.

Thickness: Steel has the largest Young's Modulus, ultimate tensile and flexural strength which shows that compared to other materials it is stronger therefore thickness of a steel chassis will be lower compared to other materials. while acetal has the smallest values, therefore larger thickness.

To select the material for chassis, compromise must be made between strength, cost and weight. The material that will be used for the chassis will be acetal as it has low density, cost and is easy to manufacture. Low density means buggy will be lighter therefore overall speed and battery life of the buggy will be higher. Low cost is important as the overall budget of project is £40, it must not be exceeded. However, acetal is not the strongest which means it will flex and bend under lower stresses than the other materials, therefore a stress and displacement analysis is required to ensure, if acetal chassis will be able to withstand the load being placed on.

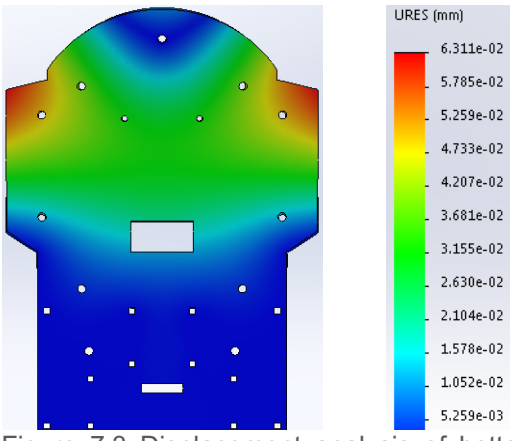

Figure 7.3 Displacement analysis of bottom plate [4]

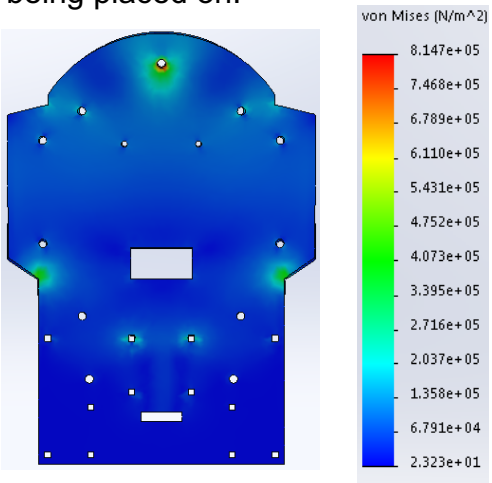

Figure 7.4 Stress analysis of bottom plate [4]

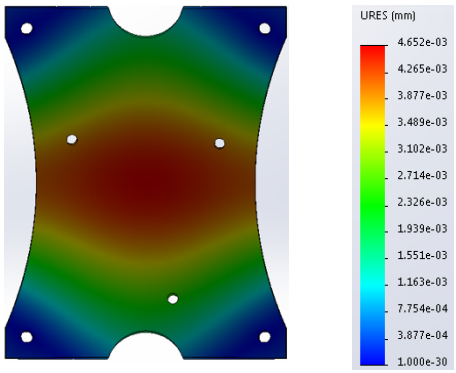

Figure 7.5 Displacement analysis of top plate [4]

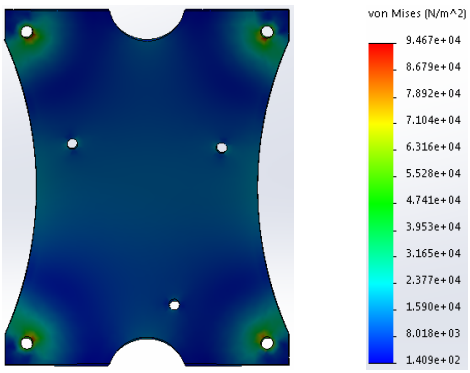

Figure 7.6 Stress analysis of top [4]

Deflection is very important as a large deflection will result in a greater bend in the chassis therefore overall driving and handling of the buggy will be affected as the wheels will not work as well and it may also interrupt the performance of the sensors. If the deflection is big enough, chassis can break. To make sure deflection is not too high, load on the chassis should be evenly distributed. As can be seen from the stress analysis, the chassis will be able to withstand the stress being applied to it , and biggest deflection of the chassis is really small(in um) e.g. biggest deflection for top plate is 4.7 um.

Another reasons for acetal being chosen is, it can be cut very easily with a laser cutter, which is what will be used to manufacture the chassis, making the progress straightforward with no hassle. Glass-reinforced laminate and aluminium also have relatively low density and can withstand larger stresses than acetal. However, it is harder to cut these materials into the desired shape due to their properties.

7.3. Design and Layout:

The overall mass of the buggy (including both plates) is 1.03 kg, which is close to what was expected. Rear wheel drive (RWD) is preferred to the front wheel drive as having RWD will improve the handling and overall balance of the buggy. Smaller the size of the buggy easier to manoeuvre therefore to make the size of chassis smaller in length the chassis will consist of two plates, upper and lower, which will be connected using spacers, of required length.

Gearbox, caster ball and PCB for the sensor circuit would fit on the underside of the lower plate while motor drive board and battery pack would fit on the top side of the lower plate. Upper plate will be above the drive board and nucleo board will fit on top of it. Holes have been cut into the chassis, so every component will be screwed on the chassis except the battery pack. Velcro will be used to secure the battery pack to the chassis. Slots have been cut for the Velcro strip to thread through. For the gearbox, square holes have been cut on the chassis as the gearbox module has slots cut into it which will fit in the square holes.

Separation between the wheel will influence the buggy. Wider the wheels are the larger the deflection due to increased length of chassis therefore higher chances of it bending. Wider chassis will also increase the weight therefore reducing the speed, and there is also higher risk of buggy touching the sides of the racing track, which will have 28 cm wide pinch points. Taking all this in consideration, buggy will be 19m wide (with tyres on).

8. Summary

To summarise, this report explains what the aim of the project is, what the buggy is going to do and how. Basically, the buggy will follow a white line through some obstacles, here, extreme conditions were not assumed. It will be able to do it with a configuration of six TCRTR5000 sensors. This sensor was chosen because its sensitivity and footprint are more suitable compared to the others. They will be implemented in the form of a Y because this shape is more beneficial for sensing the curves and it was based on the PID algorithm and digital controlling theory that will be implemented. The performance of the buggy will be enhanced using other non-line sensors just as it is the AEAT-601B-F06 for measuring the speed in the wheels, the DS2781 for measuring the power in the batteries and the HM – 10 module for sending the command of turning around the buggy.

All these components will be placed on a chassis made of acetal, the weight, cost, and thickness of this material make it better than the other options. Strong enough to keep all the elements safe but it is lightweight to do not represent a problem in terms of speed. No issue was found after the analysis, this material does not bend more than expected. This ends the technical characterisation.

9. Reference

[1] STMicroelectronics (2018) *STM32F401RE* Available at: https://www.st.com/content/st_com/en/products/microcontrollers/stm32-32-bit-arm-cortex-mcus/stm32-high-performance-mcus/stm32f4-series/stm32f401/stm32f401re.html (Accessed: 04/11/2018).

[2] Available at: http://www.inpharmix.com/jps/PID_Controller_For_Lego_Mindstorms_Robots.html

[3] Available at: https://www.csimn.com/CSI_pages/PIDforDummies.html

[4] (version 2018). Solidworks: University of Manchester.

[5] (2018-2019). *ESP Technical Handbook*: University of Manchester. 84-85.

[6] (2018-2019). *ESP Procedural Handbook*: University of Manchester. 84-85.

[7]Available at: http://www.farnell.com/datasheets/1818035.pdf?_ga=2.64058409.783467778.1543460102-164713630.1539548520

[8] Available at: https://www.vishay.com/docs/83760/tcrt5000.pdf

[9] Available at: http://www.farnell.com/datasheets/1662254.pdf?_ga=2.103249798.783467778.1543460102-164713630.1539548520

[10] Available at: http://www.farnell.com/datasheets/612931.pdf

[11] Available at: https://www.vishay.com/docs/81516/bpw17n.pdf

[12] Available at: https://www.mouser.com/ds/2/311/SFH%20203,%20SFH%20203%20FA,%20Lead%20(Pb)%20Free%20Product%20-%20RoHS-319015.pdf

[13] Available at: http://www.ti.com/lit/ds/symlink/uln2003a.pdf

[14] Available at: http://www.ti.com/lit/ds/symlink/lm339.pdf

[15]Missous, M(2017) Electronic Materials (chapters 6.6 – 7.6)

[16] Altium(2016) Altium Designer 2016 (used 29/11/2018 at the University of Manchester)

[17]InParmix(2018) Available at: http://www.inpharmix.com/jps/PID_Controller_For_Lego_Mindstorms_Robots.html (Accessed: 22/11/2018)

[18]Control Solutions Minnesota (2018) Available at: https://www.csimn.com/CSI_pages/PIDforDummies.html (Accessed: 25/11/2018)

[19] Podd,F (2018-2019). ESP Technical Handbook: University of Manchester. 65

[20] Microcontroller pins definitions table 8, Available at: https://www.st.com/resource/en/datasheet/DM00086815.pdf

[21] Podd,F (2018-2019). ESP Technical Handbook: University of Manchester. 74

[22] Texas instruments (2015, September) LM3480 Datasheet Available at: http://www.ti.com/lit/ds/symlink/lm3480.pdf

[23] Drive board connections Available at: https://online.manchester.ac.uk/bbcswebdav/pid-6247170-dt-content-rid-26307173_1/courses/I3027-EEEN-21000-1181-1YR-027927/Motor%20Drive%20board%20connections%281%29.pdf

[24] microcontroller pinout https://os.mbed.com/platforms/ST-Nucleo-F401RE/#board-pinout

[25] DS2781 datasheet Available at: https://datasheets.maximintegrated.com/en/ds/DS2781.pdf

[26] martyncurrey HM-10 article http://www.martyncurrey.com/hm-10-bluetooth-4ble-modules/

[27] Podd,F (2018-2019). ESP Technical Handbook: University of Manchester. 72 – 73

[28] Liam,M (2018-2018). ESP Week 7 Lecture PWM/Motor control pg 45

[29] Available at: https://www.st.com/resource/en/user_manual/dm00105823.pdf pg 21